Mitigating elastic effects of acoustic full waveform inversion for VSP data via deep learning

He Liu, Luping Qu, Daniel Trad, and Kristopher Innanen

ABSTRACT

Full waveform inversion (FWI) is a valuable technique for estimating high-resolution subsurface physical property models. It has become a potent tool for time-lapse seismic inversion. Due to the high resolution feature of underground structures, VSP data have to used to monitor changes in reservoir profiles during activities like injection and production, as well as for long-term CO_2 storage. Nevertheless, FWI faces a significant computational burden, elastic FWI takes much more efforts than acoustic FWI, and time-lapse FWI typically involves at least two FWI computations. Source-encoding strategies can be employed to accelerate the inversion, however, they will eventually introduce crosstalk noise in the inversion results and this phenomena is more obvious in elastic cases.

Acoustic full waveform inversion is usually the first choice for velocity model building due to its efficiency and robustness. However the recorded field data always contain elastic effects due to such as PS and SP-wave conversions, even in marine acquisitions. In this work, we adopt a deep learning approach to mitigate the elastic effects in VSP data. We train convolutional network to map elastic shot gathers into their acoustic counterparts, and perform acoustic FWI using the pseudo-acoustic shot gather. Our experiments show that the transformed acoustic data can match well with the direct simulated acoustic data. And the inversion results also show improvement compared with the inversion result by acoustic FWI using elastic data.

INTRODUCTION

monitoring

Time-lapse seismic analysis is extensively employed for monitoring changes in subsurface properties, such as those arising from oil/gas production or CO_2 injection (Greaves and Fulp, 1987; Ross and Altan, 1997; Wang et al., 1998; Barkved et al., 2003; Arts et al., 2004; Barkved et al., 2005; Arts et al., 2004; Chadwick et al., 2009; Kazemeini et al., 2010; Pevzner et al., 2017). The high-resolution feature of Vertical Seismic Profile (VSP) data is attractive for seismic imaging (Daley et al., 2008). This is particularly relevant for quantifying time-lapse variations induced by CO_2 injection, which usually introduce small velocity change in the reservior area.

Full-waveform inversion (FWI) has emerged as a potent tool for the time-lapse seismic analysis, offering promising capabilities for tracking changes in reservoirs over time. FWI is a high-resolution seismic imaging technique that leverages the full information contained within seismic traces, including both amplitude and phase, to extract physical parameters of the subsurface medium probed by seismic waves (Virieux and Operto, 2009; Virieux et al., 2017), which is proposed by Tarantola (1984) in time domain to invert the subsurface P-wave velocity model by minimizing the l2-norm of the difference between predicted and observed data (Symes, 2008). Pica et al. (1990) further considered S-wave and extend FWI

into elastic cases. While in the elastic case, the cycle-skipping issue gets more challenging. Bunks et al. (1995) propose a multi-scale strategy to deal with the cycle skipping issue in FWI.

Consequently, Full-Waveform Inversion (FWI) with VSP seismic data has emerged as a promising strategy to resolve subsurface model properties and generate time-lapse images for monitoring injected CO2 plumes (Podgornova et al, 2017; Egorov et al, 2018; Eaid et al, 2020; Podgornova et al, 2022; Eaid et al, 2023).

However, FWI continues to suffer from a significant computational cost, primarily due to its iterative and computationally intensive nature. In each iteration, the objective function's gradient must be computed concerning the model parameters, accomplished by cross-correlating the backward-propagated residual wavefield with the corresponding forward-propagated source wavefield. Calculating these two types of wave fields places significant demands on computational resources, as it involves performing a substantial number of times to solve the wave equation. For time-lapse FWI, the computational cost is normally double or four times of that in 2D or 3D FWI. Therefore, there is an urgent need to reduce computational complexity for time-lapse FWI. In addition, elastic FWI considering the elastic effects further makes computational overburden more severe. Considering the Vs model makes the inversion much more complicated. And the multi-scale strategy (Bunks et al., 1995) has to incorporated, which usually takes more iterations.

In time-lapse FWI, another issue we need to consider is the time-lapse strategy. The most commonly used time-lapse FWI strategy is known as the parallel strategy (PRS) (Lumley et al., 2003; Plessix et al., 2010), in which the baseline and monitor models are independently inverted with the same initial model, and the inverted time-lapse change is the difference between two inverted models. Due to different convergence in two independent inversions, this strategy usually introduces artifacts in the final inverted time-lapse change. Consequently, a series of more advanced time-lapse strategy have been proposed, including the sequential strategy (SQS)(Routh et al., 2012), the double-difference strategy (DDS)(Zheng et al., 2011; Zhang et al., 2012; Zhang and Huang, 2013), the common-model strategy (CMS)(Hicks et al., 2016; Bortoni et al., 2021), the central-difference strategy (Zhou and Lumley, 2021). While most of these implementations in time-lapse data are based on acoustic FWI. We have expend the CMS to elastic time-lapse FWI and found out that, compared to acoustic time-lapse case, elastic effects will also degrade the time-lapse image. espectially when acquisition nonrepeatability issues and noise exsit in synthetic experiments.

A efficient way to reduce the computational time is source-encoding strategies (Romero et al., 2000; Krebs et al., 2009), which reduce the data dimension by encoding the individual shot gathers into super-shots. However, these methods will eventually introduce crosstalk noise into the inverted models.

Take into account the various factors mentioned earlier, despite the elastic nature of the earth, the wavefield is usually assumed acoustic and the acoustic wave equation is typically used to model wave propagation in FWI. This assumption is essential for being efficient, espectially conducting FWI for frequent time-lapse monitoring surveys or large scale 3D

datasets. However, neglecting the elastic effects will reduce the accuracy and resolution of the recovered P-wave velocity models, as well as a loss in potential to constrain other physical properties, such as the S-wave velocity given that amplitude information in the observed data set is not fully used. (Agulo, et al., 2018).

To deal with this problem, many researches have been conducted. Chapman et al.(2014) and Hobro et al. (2014) proposed acoustic wave equation with correction that accounts for some elastic effects. Agulo et al. (2018) have proposed to use matching filters to correct elastic data to acoustic equivalents, and then perform acoustic FWI using corrected data.The imprint of elastic effects on the recovered P-wave models is mitigated, leading to better-resolved models than those obtained after conventional acoustic FWI. It costs more than conventional acoustic FWI, but still much less than elastic FWI. Li et al. (2019) proposed to use a deep learning approach to conduct the elastic data correction. and explored different training strategies. Yao et al. (2020) applied generative adversarial networks to perform elastic data correction in data domain, and also correct acoustic FWI updates in the gradient domain. Voytan et al. (2022) extended the work by Li et al. (2019) to realistic 3D synthetic velocity model under narrow-azimuth marine streamer acquisition geometry. besides of application to offshore field data test, this work also applied a deep convolutional network to correct synthetic acoustic shot gathers to elastic equivalents.

In this work, we train a convolutional network to mitigate the elastic effects in VSP data. Following Li et al. (2019) and Voytan et al. (2022). First, we conduct acoustic full waveform inversion based on an initial Vp model, and then obtain a Vp model that we can use to as an acoustic model to generate acoustic training data. Through assumptions of Vp/Vs ratios, we can build a series of Vs models and generate elastic shot gathers for network training. The generated elastic and acoustic shot gather pairs are used as inputs and labels for the convolutional network. At last, we use the network to predict the transformed acoustic counterpart of elastic shot gather, and perform acoustic FWI with the predicted acoustic data.

METHOD

Mitigating elastic effects

Following Li et al. (2019) and Voytan et al. (2022), we train a deep convolutional network (CNN) to learn a data driven mapping between shot gathers generated in an elastic model and shot gathers in an acoustic model. We adopt the workflow proposed by Agudo. First, we assume that we have access to observed data acquired at the surface and the initial Vp model as is necessary for acoustic FWI. then we invert Vp for a few iteraion of acoustic FWI from the initial model. in this way, we can obtain an acoustic model, which will be used to simulate field data as well as build an elastic model through an assumption of Vp/Vs ratio. This estimate is based on out initial Vs model and allows for variability between subsurface structures.

After building the elastic models, we use them and the acoustic model to generate synthetic acoustic and elastic shot gather pairs under the same acquisition geometry. Then we use the data pairs to train a deep convolutional network to learn the mapping from an

elastic shot gather to an acoustic equivalent. at last, we apply the trained network to elastic observed data to perform acoustic FWI.

UNet

Training a CNN is equal to solving the following optimization problem:

$$\min_{\theta} \left\| I^{label} - G_{\theta}\left(I\right) \right\|_2^2,$$

where I^{label} and I are acoustic label data and elastic input data to be transformed, respectively (Li et al., 2019). Together they form a training dataset. The function G_{θ} is a multi-layer convolutional neural network parameterized symbolically by θ. It maps from a section in an elastic data shot gather to the corresponding part in an acoustic shot gather, which are of the same dimensionality. Following Voytan et al. (2022), in this work, we use a UNet as the training network. The architecture is shown in Fig 1. we designed the UNet with 5 encoder layers and 5 decoder layers, each of which consists of a convolutional layer, a Leaky ReLU layer, another convolutional layer and another Leaky ReLU layer, followed by a maxpool layer. The U-Net architecture has proven effective in various com-

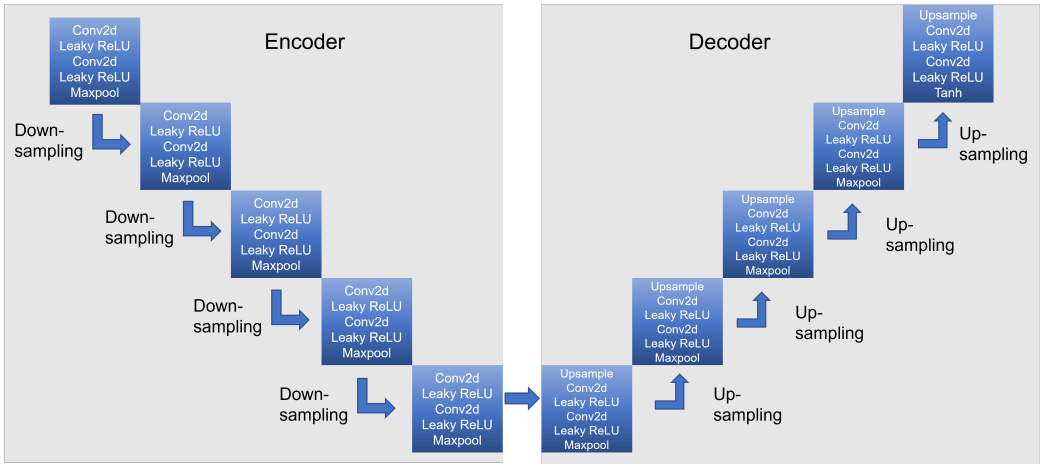

FIG. 1. Architecture of the convolutional neural network.

puter vision tasks, particularly in medical image analysis. Our U-Net architecture consists of an encoder-decoder structure with skip connections. The encoding path, also known as the contracting path, captures hierarchical features, while the decoding path, or expansive path, reconstructs the input image from these features. This enables the network to capture both low-level and high-level details.The architecture is defined as follows: Encoder Layers (Downsampling):The initial layer takes a single-channel input (e.g., grayscale image) and applies a series of convolutions and leaky ReLU activations.Subsequent layers consist of convolutional blocks followed by leaky ReLU activations and max-pooling operations, reducing spatial dimensions. Decoder Layers (Upsampling):Each decoder layer consists of an upsampling operation followed by convolutional blocks with leaky ReLU activations. Skip connections connect corresponding encoder and decoder layers to preserve fine-grained information. Output Layer:The final decoder layer outputs a single-channel image with the Tanh activation function, suitable for regression tasks.

Review of full waveform inversion in time domain

In a standard FWI problem, we minimize a misfit function

$$\mathbf{E}(\mathbf{m}), \tag{1}$$

subject to

$$\mathbf{F}(\mathbf{m})\mathbf{u}(\mathbf{x},t) = \mathbf{s}(\mathbf{x},t), \tag{2}$$

where $\mathbf{E}$ is a function with respect of model parameters $\mathbf{m}$, $\mathbf{F}(\mathbf{m})$ characterizes the seismic wave equation, $\mathbf{u}(\mathbf{x},t)$ denotes the particle displacement at time $t \in [0,T]$ excited by an external source $\mathbf{s}(\mathbf{x},t)$ and $\mathbf{x}$ denotes spatial coordinates .

The wave equation $\mathbf{F}(\mathbf{m})$ in elastic media can be expressed as (Aki and Richards, 2002)

$$\mathbf{F}(\rho,\lambda,\mu) = \rho(\mathbf{x})\frac{\partial^2}{\partial t^2}[\cdot] - \nabla\cdot\left[\lambda(\nabla\cdot[\cdot])\mathbf{I} + \mu\left(\nabla[\cdot] + \nabla[\cdot]^T\right)\right],$$

where $[\,\cdot\,]$ is a place-holder for the variable acted upon by $\mathbf{F}(\mathbf{m})$ and $\mathbf{I}$ is the identity operator. ρ, λ and μ denote density and the Lamé parameters. This elastic wave equation can be solved by the stagger-grid finite-difference scheme (Virieux, 1986; Levander, 1988). The objective function taking the least-squares norm of the misfit vector $\Delta\mathbf{u}$ is given by

$$\begin{aligned}\mathbf{E}(\mathbf{m}) &= \frac{1}{2}\Delta\mathbf{u}^\dagger\Delta\mathbf{u} = \frac{1}{2}\left\|\mathbf{u}_{\text{obs}} - \mathbf{u}_{\text{syn}}\right\|^2 \\ &= \frac{1}{2}\left(\mathbf{u}_{\text{obs}} - \mathbf{u}_{\text{syn}}\right)^{\text{T}}\left(\mathbf{u}_{\text{obs}} - \mathbf{u}_{\text{cal}}\right) \\ &= \frac{1}{2}\sum_{s=1}^{N_s}\sum_{r=1}^{N_r}\int_T \left|u_{\text{obs}}\left(\mathbf{x}_r,t\right) - u_{\text{syn}}\left(\mathbf{x}_r,t;\mathbf{m}\right)\right|^2\,\mathrm{d}t,\end{aligned} \tag{3}$$

where $\dagger$ denotes the adjoint operator (conjugate transpose), the data misfit $\Delta\mathbf{u}$ is defined by the differences between the observed seismic data $\mathbf{u}_{\text{obs}}$ and the synthetic seismic data $\mathbf{u}_{\text{syn}}$ recorded at the r-th receiver and generated by the s-th source $\mathbf{s}_s$ for model $\mathbf{m}$. N_s and N_r denote she number of sources and receivers.

Via the conjugate gradient method, the model is updated iteratively according to

$$\mathbf{m}_{k+1} = \mathbf{m}_k + \alpha_k\delta\mathbf{m}_k, \tag{4}$$

where k is the iteration number, α the step length, and $\delta\mathbf{m}_k$ is a search direction or descent direction and can be derived from the gradient of the misfit function. The gradient of $\mathbf{E}(\mathbf{m})$ with respect to $\mathbf{m}$, $\nabla_m\mathbf{E}$, can be calculated efficiently using the adjoint-state method (Plessix, 2006):

$$\nabla_m\mathbf{E}(\mathbf{x}) = -\sum_{s=1}^{N_s}\int_T u^\dagger_{\text{obs}}\left(\mathbf{x},t\right)\cdot\frac{\partial\mathbf{F}}{\partial\mathbf{m}}u_{\text{obs}}\left(\mathbf{x},t\right)\mathrm{d}t. \tag{5}$$

where $u^\dagger_{\text{obs}}$ is the adjoint wavefield.

SYNTHETIC EXAMPLES

In our study, we assume a constant density and perform EFWI for Vp and Vs using the IFOS2D software (Bohlen et al., 2016). We use a down-sampled elastic Marmousi II model to conduct experiments in EFWI. The model has a distance of 4100 m and a depth of 1500 m in a grid with a size of 410 by 150 and a 10-meter spacing. The true Vp and Vs models are plotted in Figure 2a and 2b. We employ the smoothed true models as the initial models, which are plotted in Figures 3a and 3b. There is a 200 m-thick water layer at the top of the model. The Vs model is created by prescribing a constant Vp/Vs profile that equals to 1.7 from the sea bottom to 100m deeper. Below that is a linear 1-D transition zone of another 100m, in which the ratio decreases from 3.0 to 1.7 (Fig. 4). The remaining deeper part has a constant Vp/Vs ratio that equals to p3.0. We create the density model according to the Gardner's equation:

$$\rho = 310 V_p^{0.25} \text{ kg/m}^3 \tag{6}$$

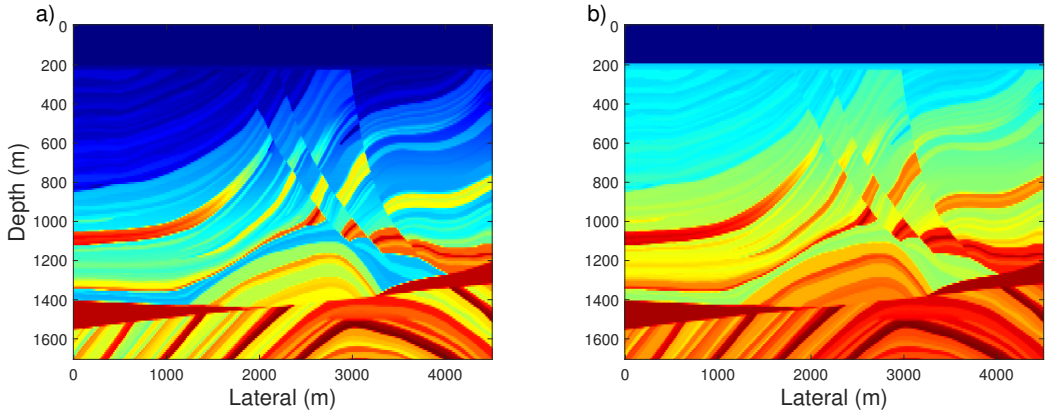

FIG. 2. True model: a) Vp model and b) Vs model.

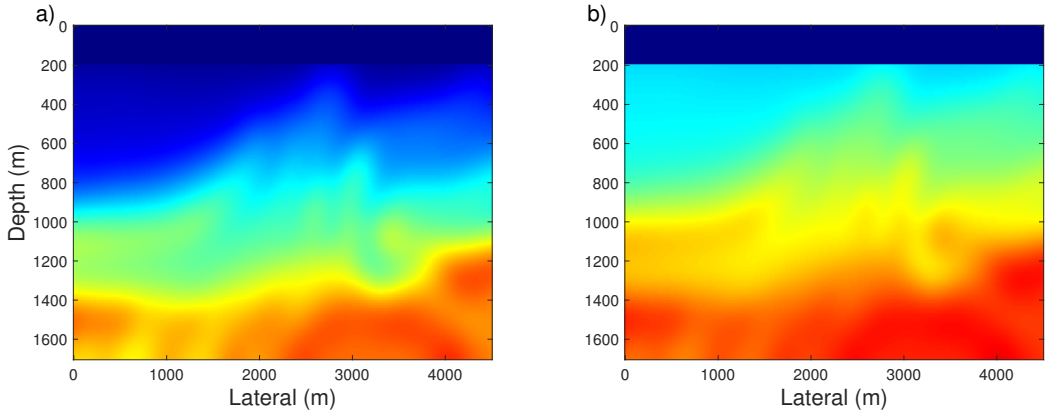

FIG. 3. The initial model: a) Vp model and b) Vs model.

Training data preparation

The training strategy is similar with the ones used by Agudo and Voytan we use training data created from results of acoustic full waveform inversion of elastic, so that the trained

networks are adjusted to the specific inversion problem. We first perform acoustic FWI of elastic data, and use the inverted model to generate a series of elastic models. Then, we use those models to compute a series of training datasets and construct a network that is relevant to the specific geology in our inversion. This is similar to the work with Wiener filters, but it differs in that we can use multiple Vp/Vs ratios and velocit ydensity relations rather than a fixed one to accommodate a wide ranges of senarios since the true model is unknown.

Each training input and label is a single shot gather of VSP data.

Network and Training

The U-Net is trained on a dataset comprising input images and corresponding ground truth masks. The loss function used during training is tailored to the specific segmentation task, and optimization is performed using stochastic gradient descent (SGD) or other suitable optimizers.

To evaluate the performance of our U-Net architecture, experiments were conducted on a dataset of size (50, 1, 2400, 128), with the model trained on [mention your training strategy, e.g., mean squared error loss] and validated on [mention your validation strategy].

The training problem is solved by the gradient-based optimization method ADAM (Kingma and Ba, 2014) with a learning rate of 1e-4. The Mean Squared Error (MSE) loss function is chosen to quantify the difference between predicted and ground truth labels.The mean-squared-error (MSE) relative to the true model, defined as

$$\mathrm{MSE}\left(M^{\mathrm{true}}, M^{\mathrm{inv}}\right) = \frac{1}{N_z N_x} \sum_{i=1}^{N_z} \sum_{j=1}^{N_x} \left(M_{ij}^{\mathrm{true}} - M_{ij}^{\mathrm{inv}}\right)^2 \tag{7}$$

Results

We first examine the full waveform inversion results using VSP configuration, we respectively perform acoustic FWI using acoustic data, elastic FWI using elastic data, and acoustic FWI using elastic data. The inverted result comparison is displayed in Fig 4. From this figure, we can notice that the elastic effects are so severe in the VSP data inversion. There's so much information lost in the inverted model, we can barely generate training data with meaningful information based the acoustic inversion result using elastic data. In addition, we consider there is only one VSP well for acquiring data, the aperture is very limited.

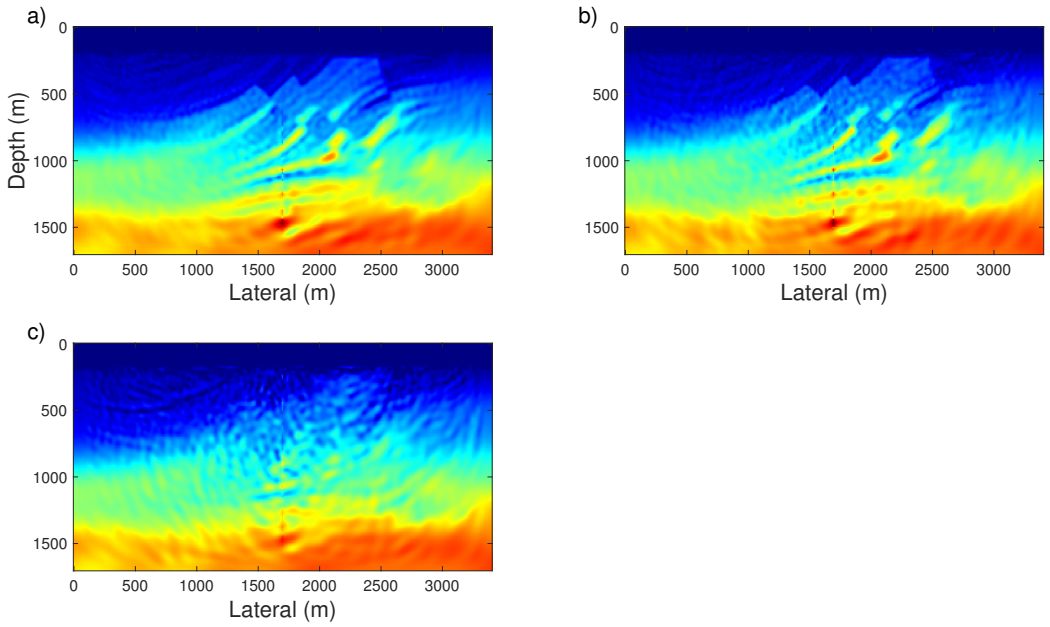

FIG. 4. Full waveform inversion results using a VSP configuration a) acoustic FWI using acoustic data, b) elastic FWI using elastic data and c) acoustic FWI using elastic data.

Thus, we consider to perform FWI using a surface acquision geometry. Similarly, we perform FWI using different data and examine the elastic effects. The inversion result comparison is shown in Fig 5. Compared with Fig 4, we can obtain much more subsurface information from the inverted model by acoustic FWI using elastic data. Based on this inverted model, we can build a Vp model with better aperture and resolution. Consider a VSP configuration, we shorted the lateral dimension of the model, and obtain a Vp model with dimension 170 by 240.

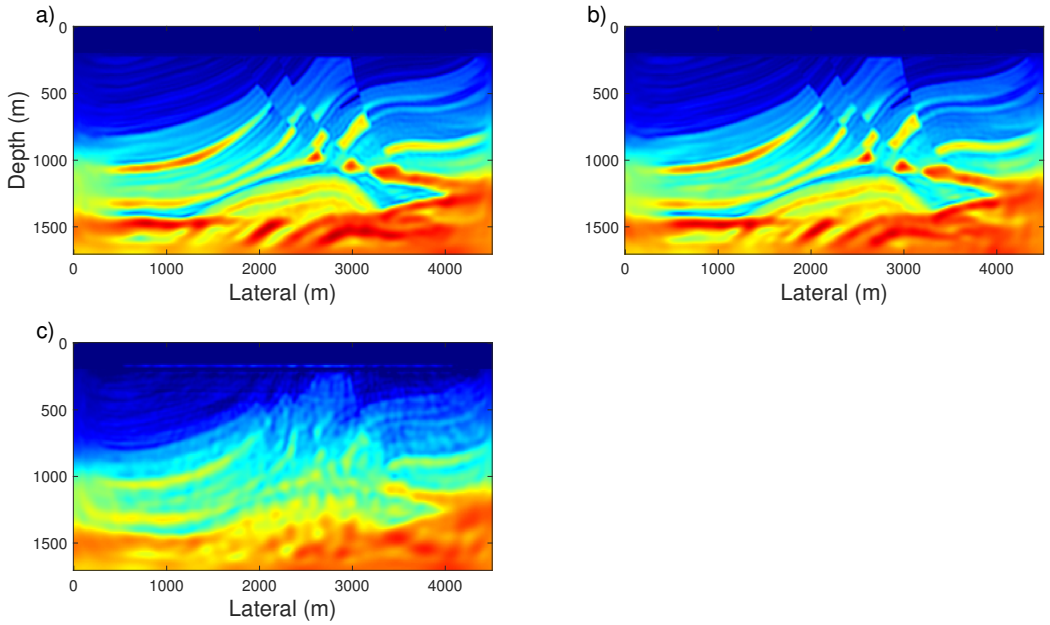

FIG. 5. Full waveform inversion results using a surface configuration a) acoustic FWI using acoustic data, b) elastic FWI using elastic data and c) acoustic FWI using elastic data.

Then we proceed with inverted Vp model and create Vs models with different Vp/Vs ratios (1.6, 1.65, 1.7, 1.75, 1.8) above the transition zone. The depth of the transition zone is the same as in the true model and Vp/Vs ratio is 1.7 below the transition zone. In our VSP data acquisition geometry, there are 300 shots that are 20 m deep in the water with a 10 m shot interval, and 128 receivers in the acquisition well located from 220 m deep with a 10 m receiver interval. The source time function is a Ricker wavelet with a central frequency of 10 Hz. Overall, we model 1500 acoustic shot gathers and 1500 elastic shot gathers. To build training and validation datasets, we select every 30th shot for testing. We train 2400 images and reserve 500 for validation. The amplitude of the Ricker wavelet it adjusted, so the amplitude of generated shot gathers are between -1 to 1.

In Fig 6, we display the shot gathers generated by acoustic and elastic models. The differences between acoustic and elastic wave propagation are particulary pronounced on top of structures where large shear impedance contrasts cause a significant fraction of energy to partition into S-wave conversion. Compared with the acoustic shot gather shown in Fig 6a, there shows clear S-wave conversion energy in the elastic shot gather. And it dominates the energy difference shown in Fig 6c. All sub figures are displayed under the same scale.

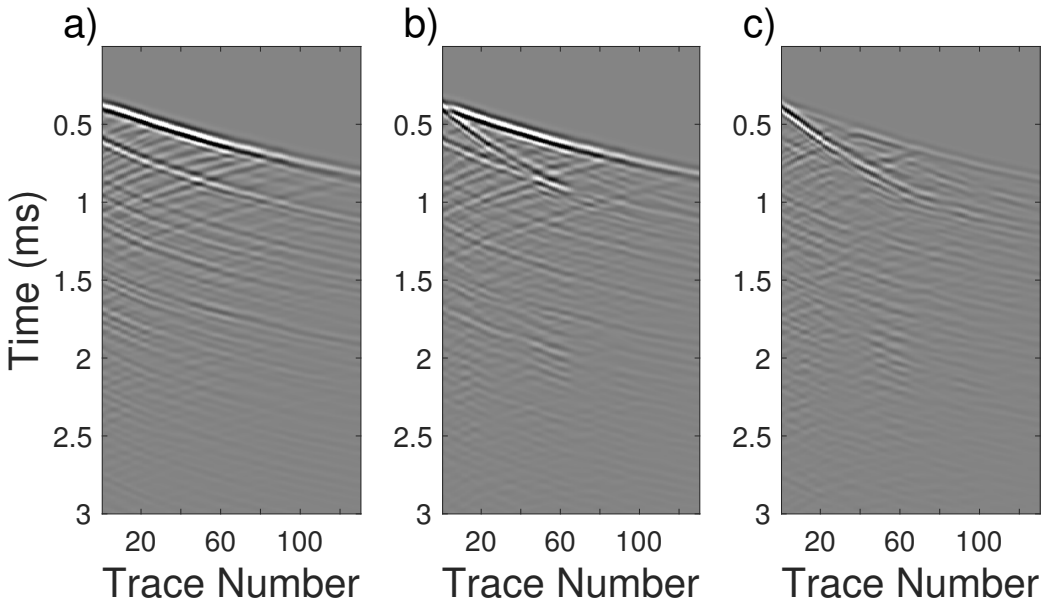

FIG. 6. Simulated shot gathers from Marmousi model a) acoustic VSP data, b) elastic VSP data, and c) the difference.

The deep learning algorithm is implemented in the PyTorch framework, parallelized on one NVIDIA a100 GPU inside one node. It usually takes around 25 mins to complete one epoch with 2400 training data. The total time to train one network from scratch is around 3 hours. The training loop is executed for a total of 1000 epochs. For each epoch, the U-Net is trained on batches of seismic images and corresponding labels. The training loss is computed using the MSE loss function.To monitor the model's generalization performance, a validation loop is implemented at regular intervals (every 5 epochs).This process is conducted without gradient computation to speed up the evaluation. In Fig 7, we present the train and validation loss curves.

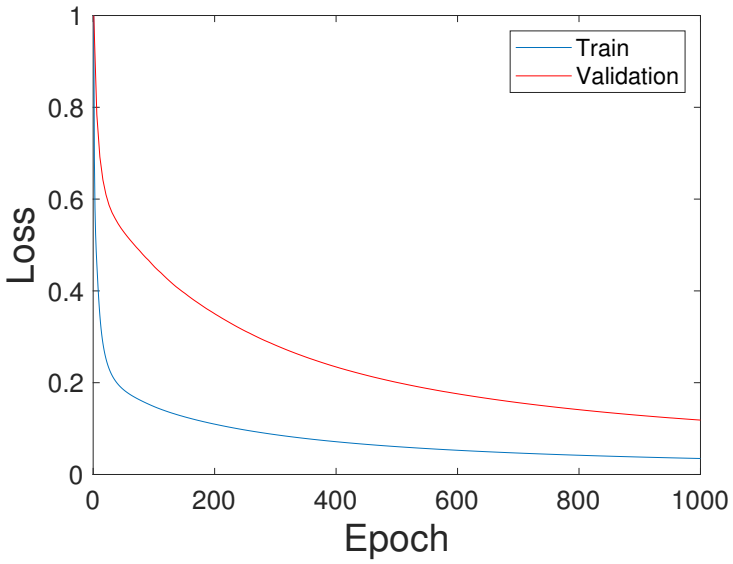

FIG. 7. Train and validation loss

We transform the elastic data with the network trained using the above training data shown in Fig 6. In Fig 8 and 10, we present the predicted acoustic shot gathers when the source is excited in the middle and middle right of the model. In Figure a) to c) are the elastic input data, acoustic label data and predicted transformed acoustic data. In Figure d) to e), we compare the difference between input and label, input and prediction, label and prediction, respectively. Displayed under the same scale, we can notice that the trained network can well mapping the elastic shot gathers into the acoustic counterparts.

In Fig 9 and 9, we also compare the spectra in both cases. From the comparisons, we can see that the spectrum of predicted data can match well with the label data at most frequencies, except below around 5 Hz.

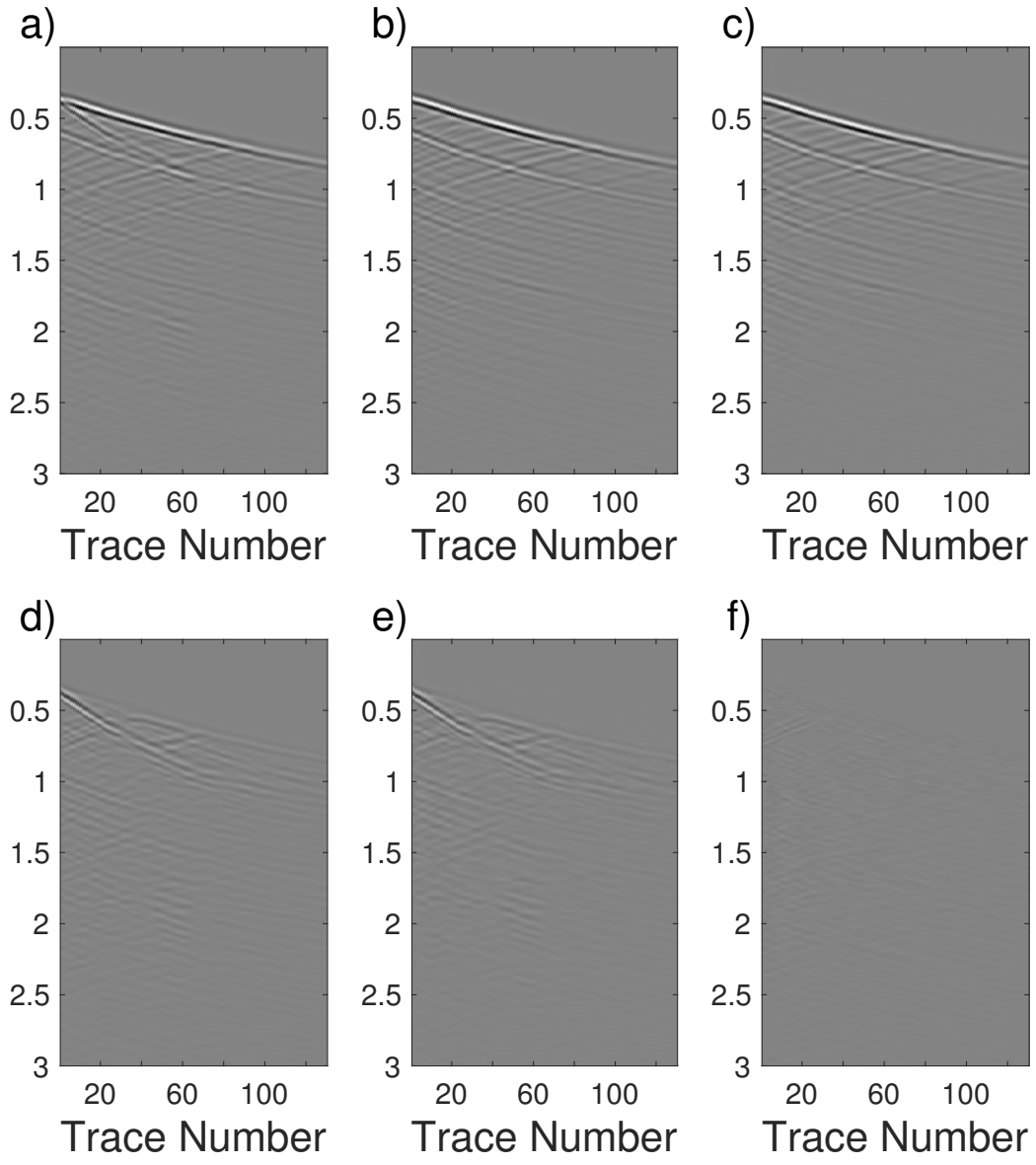

FIG. 8. Simulated shot gathers from Marmousi model a) acoustic VSP data, b) elastic VSP data, and c) the difference

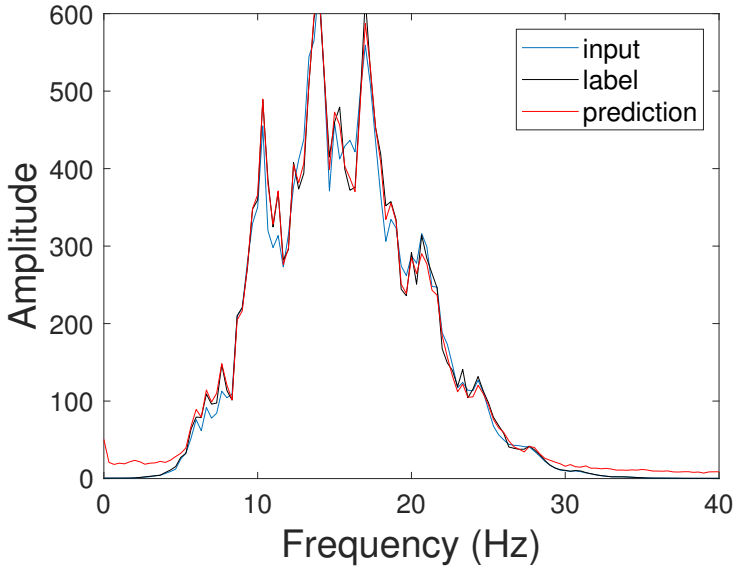

FIG. 9. Spectra comparison between elastic, acoustic and transformed acoustic shot gathers.

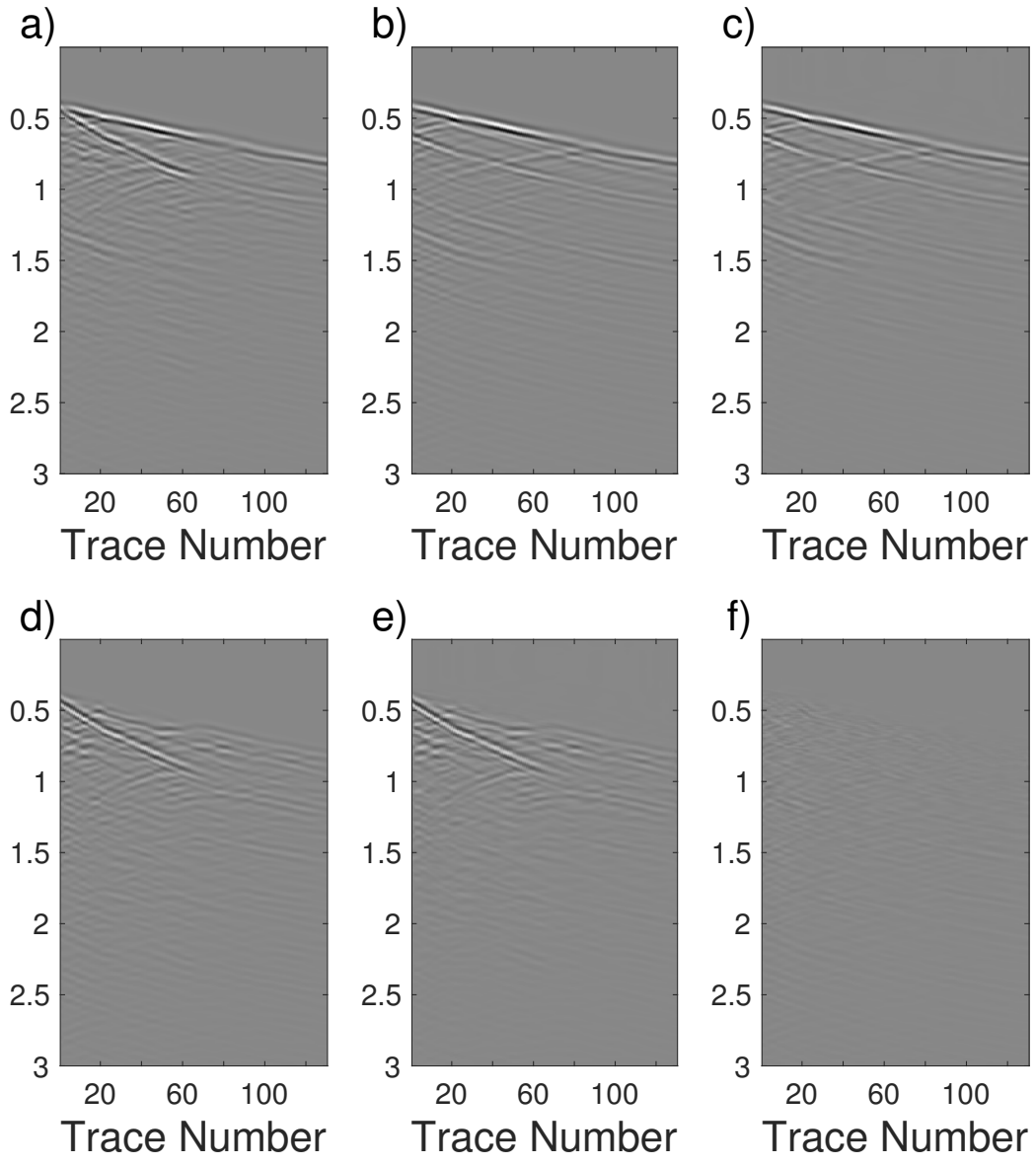

FIG. 10. Simulated shot gather from Marmousi model a) acoustic VSP data, b) elastic VSP data, and c) the difference

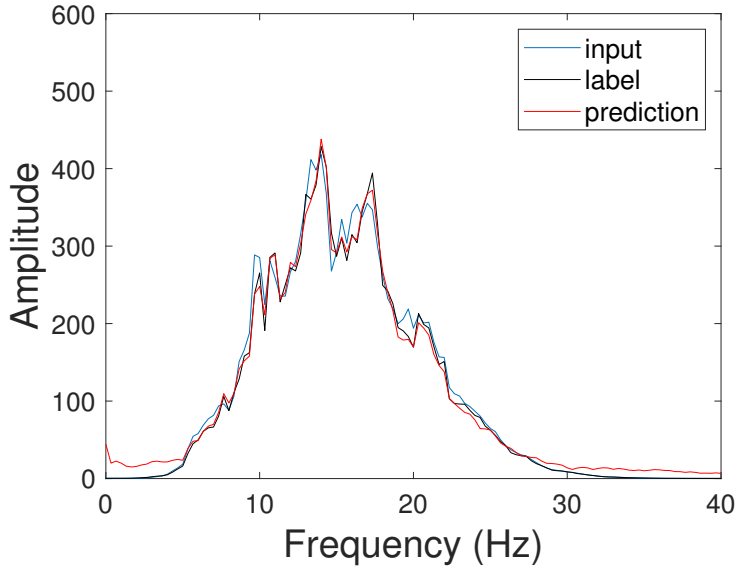

FIG. 11. Spectra comparison between elastic, acoustic and transformed acoustic shot gathers.

Then we conduct acoustic FWI using transformed acoustic data. To avoid the mismatch of data at low frequency, we perform multi-scale FWI starting above 5 Hz. The inverted result is shown in Fig 12, we can notice it has fewer elastic effects and exhibits much improved inversion. The structures are better recovered, especially, the deeper part of the model has higher resolution than the elastic data result.

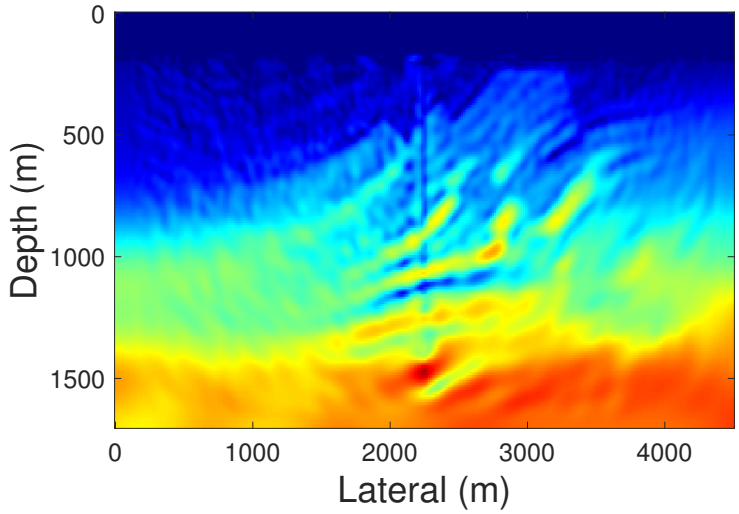

FIG. 12. Acoustic full waveform inversion result using transformed acoustic data.

CONCLUSIONS

We develop a deep convolutional network to correct VSP seismic data to mitigate elastic artifacts in acoustic full waveform inversion of geophone VSP data. In this work, we implemented and tested a deep-learning approach of using convolutional neural networks to reduce elastic effects in observed VSP data for acoustic FWI. Our synthetic tests show

that elastic wave phenomena can be effectively suppressed by the deep learning approach and the models from acoustic FWI were significantly improved by using the transformed elastic dataset. We use a series of models constructed from acoustic inversion of elastic data to forward simulate training data related to the model to be inverted for. this method can decrease the computational cost and improve the the monitoring efficiency.

ACKONWLEDGEMENT

The sponsors of CREWES are gratefully thanked for continued support. This work was funded by CREWES industrial sponsors, NSERC (Natural Science and Engineering Research Council of Canada) through the grant CRDPJ 543578-19.

REFERENCES

Aki, K., and Richards, P. G., 2002, Quantitative seismology: San Francisco: University Science Books.

Arts, R., Eiken, O., Chadwick, A., Zweigel, P., Van der Meer, L., and Zinszner, B., 2004, Monitoring of co2 injected at sleipner using time-lapse seismic data: Energy, **29**, No. 9-10, 1383–1392.

Barkved, O., Buer, K., Halleland, K., Kjelstadli, R., Kleppan, T., and Kristiansen, T., 2003, 4d seismic response of primary production and waste injection at the valhall field, *in* 65th EAGE Conference & Exhibition, EAGE Publications BV, cp–6.

Barkved, O. I., Kristiansen, T., and Fjær, E., 2005, The 4d seismic response of a compacting reservoir-examples from the valhall field, norway., *in* 2005 SEG Annual Meeting, OnePetro.

Bohlen, T., De Nil, D., Köhn, D., and Jetschny, S., 2016, Sofi2d seismic modeling with finite differences: 2d—elastic and viscoelastic version: user guide.

Bortoni, S., Barragan, S., Azevedo, G., Cypriano, L., Ferreira, A., Moreira, W., dos Reis, P. et al., 2021, Learnings from an fwi imaging study using 3d and 4d data over a postsalt field in campos basin, *in* SEG/AAPG/SEPM First International Meeting for Applied Geoscience & Energy, OnePetro.

Bunks, C., Saleck, F. M., Zaleski, S., and Chavent, G., 1995, Multiscale seismic waveform inversion: Geophysics, **60**, No. 5, 1457–1473.

Chadwick, R., Noy, D., Arts, R., and Eiken, O., 2009, Latest time-lapse seismic data from sleipner yield new insights into co2 plume development: Energy Procedia, **1**, No. 1, 2103–2110.

Daley, T. M., Myer, L. R., Peterson, J., Majer, E., and Hoversten, G., 2008, Time-lapse crosswell seismic and vsp monitoring of injected co 2 in a brine aquifer: Environmental Geology, **54**, 1657–1665.

Greaves, R. J., and Fulp, T. J., 1987, Three-dimensional seismic monitoring of an enhanced oil recovery process: Geophysics, **52**, No. 9, 1175–1187.

Hicks, E., Hoeber, H., Houbiers, M., Lescoffit, S. P., Ratcliffe, A., and Vinje, V., 2016, Time-lapse full-waveform inversion as a reservoir-monitoring tool—a north sea case study: The Leading Edge, **35**, No. 10, 850–858.

Kazemeini, S. H., Juhlin, C., and Fomel, S., 2010, Monitoring co2 response on surface seismic data; a rock physics and seismic modeling feasibility study at the co2 sequestration site, ketzin, germany: Journal of Applied Geophysics, **71**, No. 4, 109–124.

Krebs, J. R., Anderson, J. E., Hinkley, D., Neelamani, R., Lee, S., Baumstein, A., and Lacasse, M.-D., 2009, Fast full-wavefield seismic inversion using encoded sources: Geophysics, **74**, No. 6, WCC177–WCC188.

Levander, A. R., 1988, Fourth-order finite-difference p-sv seismograms: Geophysics, **53**, No. 11, 1425–1436.

Lumley, D., Adams, D. C., Meadows, M., Cole, S., and Wright, R., 2003, 4d seismic data processing issues and examples, *in* SEG Technical Program Expanded Abstracts 2003, Society of Exploration Geophysicists, 1394–1397.

Pevzner, R., Urosevic, M., Popik, D., Shulakova, V., Tertyshnikov, K., Caspari, E., Correa, J., Dance, T., Kepic, A., Glubokovskikh, S. et al., 2017, 4d surface seismic tracks small supercritical co2 injection into the subsurface: Co2crc otway project: International Journal of Greenhouse Gas Control, **63**, 150–157.

Pica, A., Diet, J., and Tarantola, A., 1990, Nonlinear inversion of seismic reflection data in a laterally invariant medium: Geophysics, **55**, No. 3, 284–292.

Plessix, R.-E., 2006, A review of the adjoint-state method for computing the gradient of a functional with geophysical applications: Geophysical Journal International, **167**, No. 2, 495–503.

Plessix, R.-E., Michelet, S., Rynja, H., Kuehl, H., Perkins, C., de Maag, J., and Hatchell, P., 2010, Some 3d applications of full waveform inversion, *in* 72nd EAGE Conference and Exhibition-Workshops and Fieldtrips, European Association of Geoscientists & Engineers, cp–162.

Romero, L. A., Ghiglia, D. C., Ober, C. C., and Morton, S. A., 2000, Phase encoding of shot records in prestack migration: Geophysics, **65**, No. 2, 426–436.

Ross, C. P., and Altan, M. S., 1997, Time-lapse seismic monitoring: Some shortcomings in nonuniform processing: The Leading Edge, **16**, No. 6, 931–937.

Routh, P., Palacharla, G., Chikichev, I., and Lazaratos, S., 2012, Full wavefield inversion of time-lapse data for improved imaging and reservoir characterization, *in* 2012 SEG Annual Meeting, OnePetro.

Symes, W. W., 2008, Migration velocity analysis and waveform inversion: Geophysical prospecting, **56**, No. 6, 765–790.

Tarantola, A., 1984, Inversion of seismic reflection data in the acoustic approximation: Geophysics, **49**, No. 8, 1259–1266.

Virieux, J., 1986, P-sv wave propagation in heterogeneous media: Velocity-stress finite-difference method: Geophysics, **51**, No. 4, 889–901.

Virieux, J., Asnaashari, A., Brossier, R., Métivier, L., Ribodetti, A., and Zhou, W., 2017, An introduction to full waveform inversion, *in* Encyclopedia of exploration geophysics, Society of Exploration Geophysicists, R1–1.

Virieux, J., and Operto, S., 2009, An overview of full-waveform inversion in exploration geophysics: Geophysics, **74**, No. 6, WCC1–WCC26.

Wang, Z., Cates, M. E., and Langan, R. T., 1998, Seismic monitoring of a co 2 flood in a carbonate reservoir; a rock physics study: Geophysics, **63**, No. 5, 1604–1617.

Zhang, Z., and Huang, L., 2013, Double-difference elastic-waveform inversion with prior information for time-lapse monitoring: Geophysics, **78**, No. 6, R259–R273.

Zhang, Z., Huang, L., and Lin, Y., 2012, Double-difference elastic-waveform inversion with weighted gradients for monitoring egs reservoirs, *in* Thirty-Seventh Workshop on Geothermal Reservoir Engineering, Stanford University California.

Zheng, Y., Barton, P., and Singh, S., 2011, Strategies for elastic full waveform inversion of time-lapse ocean bottom cable (obc) seismic data, *in* SEG Technical Program Expanded Abstracts 2011, Society of Exploration Geophysicists, 4195–4200.

Zhou, W., and Lumley, D., 2021, Central-difference time-lapse 4d seismic full-waveform inversioncentral-difference fwi: Geophysics, **86**, No. 2, R161–R172.